Supporting Information for:

Three-dimensional Quantitative Structure-Activity Relationship of Nucleosides Acting at the A_3 Adenosine Receptor: Analysis of Binding and Relative Efficacy

Soo-Kyung Kim and Kenneth A. Jacobson

Contents:

Figure III. The CoMSIA maps of the CoMSIA-2 (A) the CoMSIA-EFF (B) model. Cl-IB-MECA **68** was used as a representative ligand for the hydrophobic map. The visualization of the CoMSIA map has been performed using the StDev*Coefficient mapping option contoured by contribution. Favored and disfavored levels fixed at 80% and 20%, respectively, were used for all fields. In the CoMSIA result, the hydrophobic maps are shown in yellow for regions tolerating groups of increased hydrophobic interactions and white for regions unfavoring hydrophobic groups and favoring hydrophilic groups to increase the binding affinity to the A_3AR.

Supporting results.

Generation of data sets. To achieve a statistically significant 3D-QSAR model, the following conditions are considered generally standard: (1) a minimum range of three log units for compound binding affinity, (2) ~20 compounds (corresponding to ~5 compounds per principal component) for model generation, and (3) even distribution of the biological activities of the compounds.[22] Biological data was derived from several studies[14–21] that used the same assay conditions and radiolabeled competitive binding agonist, [^{125}I]-I-AB-MECA. Thus, the combined data set exhibited a four-log-unit difference between the highest (**72**: pK_i = 9.55) and the lowest (**71**: pK_i = 5.37) binding affinities, with other affinities evenly distributed in that range.

3D-QSAR modeling. The cross-validated q^2 is generally proving to be a much better indicator than r^2 of the reliability of a given predictions. The q^2 is generally somewhat lower, and often much lower than the conventional r^2 value. According to the CoMFA manual, the 95% confidence limit for a q^2 in CoMFA is ~0.3, so statistical significance is unlikely to be the issue. Since one or more unique compounds whose target values are badly predicted are involved in the analysis, cross-validation highlights the potential risks involved in relying on the properties of a single compound, affecting the dramatic decrease of q^2 value. Thus, we calculated q^2 value of each model and increased its value up to >0.5 through omitting an outlier in the residual plot.

To examine the predictability of the training set, preliminary 3D-QSAR studies were carried out for all 91 compounds on the basis of the binding affinity for the A_3AR subtype with SAMPLS to improve the efficiency and the speed of the 3D-QSAR. A further leave-one-out cross-validation implemented in PLS analysis was performed, in which each compound was systematically excluded from the training data set. To reduce cross-correlated brown noise in the data matrix, region focusing was applied to each model for a selective weighting of the grid points in a region. Only CoMFA (CoMFA-RF1/2) models resulted in an increase of r^2 value; other models did not (data not shown). In concert with q^2, the predictive r^2 is used to evaluate the overall performance of a model by comparing the accuracy of a series of predictions with the experimentally determined data for a given target property. The power of each model to make predictions for the A_3AR agonists was validated by using the external test sets. Comparison of the experimentally observed and predicted pKi values at the A_3AR further confirmed the predictive ability of each model. The residuals between corresponding values

of the experimental and predicted binding affinity for each compound were less than one log unit, and all test set compounds followed the regression trend line.

Although traditional CoMFA models exhibited statistical significance comparable to CoMSIA models in the present case, additional hydrophobic and H-bonding fields from CoMSIA give more information on the binding site and receptor activation, which may prove useful for the design of agonists with higher binding affinity. Since the different lattice spacing did not affect the statistical parameters of CoMSIA, one model for the relative efficacy at the A_3AR was generated with the default value of 2.0 Å lattice spacing. Since the active conformation of adenosine is unknown, the same alignment of the A_3AR-bound conformation was used for the generation of CoMSIA-EFF model.

The steric and electrostatic maps from the CoMFA-RF1 model and the hydrophobic and H-bonding maps from the CoMSIA-2 model were represented as contour maps for each property in **Figure 3**. The CoMSIA steric and electrostatic maps agreed with the CoMFA steric and electrostatic maps (Figure III-A).

Comparison of 3D-QSAR with docking models and activation mechanisms. Brief docking results of hA_3AR follows. The amine of the N^6 substituent in proximity to N250 (6.55) was H-bonded with the hydroxyl group of S247 (6.52). The 2′-OH group of the ribose ring was involved in H-bonding with the side chain of Q167 (EL2). The 3′-OH group formed a HB with the side chain of H272

(7.43), consistent with our A_3 neoceptor model.[26] The 5′-amide NH group formed an intramolecular HB with the 4′-O atom and was close to T94 (3.36), and the 5′-carbonyl oxygen atom formed a HB with S271 (7.41). The aromatic portion of the N^6-benzyl moiety showed additional π-π stacking interaction with the aromatic ring of F168 (EL2).

Previously, the activation of the human A_3AR by several adenosine derivatives was studied in intact CHO cells stably expressing this receptor.[19] SAR studies showed that small N^6-alkyl groups increased binding affinity, while bulkier aliphatic rings lowered both efficacy and binding affinity at the hA_3AR. For example, efficacy was 100% (K_i of hA_3: 6.4 nM), 97% (K_i of hA_3: 72 nM), 76% (K_i of hA_3: 73 nM), and 49% (K_i of hA_3: 411 nM) for N^6-cyclobutyl–, N^6-cyclopentyl–, N^6-cyclohexyl–, and N^6-cyclooctyl–substituted adenosine, respectively. Although selectivity for the hA_3AR was obtained with the introduction of a 3-iodobenzyl substituent at the N^6 position, N^6-(3-iodobenzyl)–substituted adenosine exhibited partial agonistic effects at the same receptor. This result is consistent with the presence of the map that requires a less sterically bulky group at the N^6 position in the CoMSIA-EFF model. Unlike in the N^6-binding site, in the binding site for C2 substituents, the presence of sterically bulky aliphatic groups, i.e. those with an increased size and chain length (compounds **3** to **7**), were tolerated with respect to maximal efficacy at the hA_3AR, correlating with the map that required a large bulky group from the CoMSIA-EFF model.

In addition, as shown in the steric and hydrophobic maps (Figure III-B), large green steric and yellow hydrophobic contours indicating tolerance of steric bulk and hydrophobicity, respectively, around the N^6-aromatic group matched well with the hydrophobic binding site surrounded by F168 (EL2), M177 (5.38), and F182 (5.43).

The appearance of red polyhedra at the meta position of the phenyl ring of the N^6 group was consistent with the observation that the electron-withdrawing groups having partial negative charge at this position in compounds **64** (N^6-3-Cl-benzyl) and **65** (N^6-3-I-benzyl) improved binding affinity in comparison with N^6-benzyl in **62** or N^6-3-methylbenzyl in **63**. Blue CoMSIA-2 contour maps requiring a positively charged group at the C2 position of the adenine ring predicted positively charged C2 substituents to increase the binding affinity at the A_3AR.

The H-bonding field map was very useful because of the importance of H-bonding of adenosine analogues in binding to the hA_3AR, especially at the ribose-binding position and at the exocyclic amine of the adenine ring. An H-bonding field was detected in the CoMSIA-EFF model near the N^6 and 5′ positions. An H-bonding donor contour around the N^6 position was directed toward the side chain of S247 (6.52), which formed a HB with the N^6H in the docking complex. Both a region requiring a HB donor at the 5′-NH and a region requiring an acceptor at the 5′-CO group from the CoMSIA-EFF model were located at the side chains of T94 (3.36) and S271 (7.41) in the putative binding site.

In a previous pharmacophore study, A_3AR-selective agonists required more H-bonding ability than did the pharmacophore of A_3AR-selective antagonists.[23] This pharmacophore study is also consistent with the receptor docking of the agonist, which showed additional H-bonding to the ribose moiety, and with the H-bonding map from the CoMSIA model.

Although there is no global active-state model, local conformational changes have been proposed.[23] In agonist-binding domains, compared with antagonist-binding domains, additional interactions were present at the kink site of TM6 and near TM7. The distinct binding sites might have differing effects on the conformational change of activation.

Table I. Binding affinities of adenosine derivatives (training set) at human (unless noted, r – rat) A_1, A_{2A}, and A_3ARs expressed in CHO cells (expressed as K_i value or percent inhibition at 10 μM unless noted) and relative maximal agonist efficacy at 10 μM at the A_3AR. Unless noted, R_1, R_2 = H; R_3 = OH; R_4 = O; R_5 = CH_2OH.

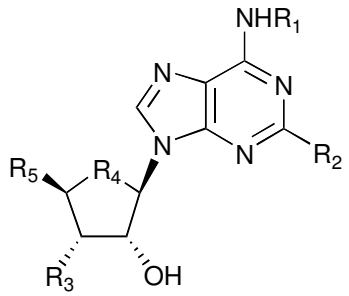

#	Substitution					AR binding affinity (nM)[a] or % displ. at 10 μM; A_3AR efficacy				Ref.
	R_1	R_2	R_3	R_4	R_5	K_i (hA_1AR)	K_i ($hA_{2A}AR$)	K_i (hA_3AR)	Efficacy (%)[b]	
1						310	700	290	ND)	39
2		Cl				7.5±1.4	630±220	87±24	100±7)	14
3		MeO				155±32	970±310	156±37	75.2±5.1)	16
4		EtO				2640±540	360±139	568±205	99.1±4.2)	16
5		*i*-PrO				16.0%	927±204	457±154	101±5)	16
6		PenO				2430±620	6.9±1.3	222±68	92.8±13.4)	16
7		*i*-PenO				4410±1150	222±89	84.2±8.4	108±10)	16
8		HexO				1830±340	156±89	124±28	43.7±6.3)	16
9		PhO				5140±1110	44±12	364±96	32.2±3.5)	16
10		BnO				642±79	585±155	117±8	16.9±3.9)	16

#	Substitution					AR binding affinity (nM)[a] or % displ. at 10 μM; A_3AR efficacy				Ref.
	R_1	R_2	R_3	R_4	R_5	K_i (hA_1AR)	K_i ($hA_{2A}AR$)	K_i (hA_3AR)	Efficacy (%)[b]	
11		PhEtO				221±57	9.3±2.9	54.2±14.3	70.7±2.7	16
12		2-MePhEtO				396±83	17.4±7.4	214±47	7.3±6.0	16
13		3-MePhEtO				295±8	41.6±22.0	242±55	70.9±3.9	16
14		4-MePhEtO				1250±250	118±95	470±81	95.5±15.1	16
15		2-MeOPhEtO				490±114	274±142	940±354	3.6±6.7	16
16		3-MeOPhEtO				246±34	32.1±1.6	231±53	85.1±5.8	16
17		4-MeOPhEtO				288±22	64.3±7.8	105±20	91.9±9.2	16
18		2-ClPhEtO				366±33	17.9±6.1	144±22	1.4±2.7	16
19		3-ClPhEtO				372±116	11.5±5.3	41.0±7.8	31.0±7.0	16
20		4-ClPhEtO				331±51	58.5±8.0	116±23	69.0±6.3	16
21		1-NaphEtO				220±18	3.8±1.4	205±19	12.8±5.9	16
22		2,2-diPhEtO				38.5%	310±119	53.6±10.4	0.0±0.6	16
23		PhEtNH				530±88	62.0±17.6	310±163	72.0±3.2	16
24					EtNHCO	6.8±2.4	2.2±0.6	16.0±5.4	100	16
25			S			5240±740	5740±980	445±54	0	17
26	Me					5970±2030	17%, 10^{-5} M	9.3±0.4	96±3	15
27	MeO					223±32 (r)	>10,000 (r)	28.6±4.7	107±13	19
28	Et					4.9±0.2 (r)	8900±770 (r)	4.7±1.9	102±6	19
29	*i*-Pr					1.9±0.1 (r)	2030±510 (r)	18.3±5.5	111±4	19
30	$(CH_3)_2CH)_2CH$					3.8±0.8 (r)	2170±490 (r)	3760±840	21±2	19

#	Substitution					AR binding affinity (nM)[a] or % displ. at 10 μM; A_3AR efficacy				Ref.
	R_1	R_2	R_3	R_4	R_5	K_i (hA_1AR)	K_i ($hA_{2A}AR$)	K_i (hA_3AR)	Efficacy (%)[b]	
31	cyclopentyl					1.8±0.5	820±216	72±12	99±6	16
32	(*S*)-*endo*-2-norbornyl					0.34±0.06 (r)		915±299	23±10	19
33	cycloPrMe					0.8±0.3 (r)	1370±410 (r)	10.2±4.1	108±4	19
34	Ph					3.3±0.3 (r)	663 (r)	14.9±3.1	102±9	19
35	Bn					77.8±6.5	2180±670	41.3±5.3	55±3	14
36	PhEt					12.9±2.1	676±39	2.1±0.4	84±5	14
37	PhEtO					225±45 (r)	>10,000 (r)	88.7±7.4	73±6	19
38	2-MeBn					59.6±14.3 (r)	24.1±1.8 (r)	47.2±10.8	100±3	19
39	2-MeOBn					36±2 (r)	761±460 (r)	32.5±4.6	81±8	19
40	2-ClBn					17±3 (r)	93±16 (r)	17.3±3.2	95±1	19
41	3-ClBn					45±3 (r)	>10,000 (r)	4.4±1.7	80±3	19
42	4-ClBn					61±3 (r)	5120±1230 (r)	47.5±4.1	96±2	19
43	(*R*)-1-Ph-2-Pr					2.04	859	8.7±0.9	102±6	14
44	*S*)-1-Ph-2-Pr					75	7780	68±12	97±3	14
45	(1*S*,2*R*)-2-Ph-1-cycloPr					30.1±6.1	2250±430	0.63±0.17	117±9	14
46	(1*R*, 2*S*)-2-Ph-1-cycloPr					15.6±1.7	2340±330	24.1±10.9	87±4	14
47	(*R*)-2-Ph-1-Pr					4.0±1.3	325±85	9.1±0.3	99±4	14
48	2,2-diPhEt					49.9±16.2	510±49	3.9±0.7	0	14
49	3,5-diMeOPh-2-MePhEt					168±29	153±26	106±22	0	14
50	9-fluorenemethyl					14.0±4.0	145±26	0.91±0.38	99±6	14

#	Substitution					AR binding affinity (nM)[a] or % displ. at 10 μM; A_3AR efficacy				Ref.
	R_1	R_2	R_3	R_4	R_5	K_i (hA_1AR)	K_i ($hA_{2A}AR$)	K_i (hA_3AR)	Efficacy (%)[b]	
51		4-CO_2HEt PhEtNH			EtNHCO	1570±460	8.8±1.6	114±16	98±5	16
52		Cl		S				4.9±1.3	64±18	17
53	Me	CN				69.8±4.4	23%	3.4±0.8	101±7	15
54	Me	NH_2				484±22	15%	39.0±2.4	98±3	15
55	Me	N_3				232±10	22.9%	10.8±3.1	83.7	21
56	Me	4-MePhC≡C				2560±610	29%	1.5±0.4	9.4	21
57	Me	4-PenPhC≡C				5.2%	6.2%	33.3±0.2	0	21
58	Me	4-Ph-triazole				35.8%	4.6%	14.9±1.7	14.0	21
59	Me	4-Bn-triazole				589±55	19.9%	9.5	0	21
60	Me	4-(4-PrO-Ph)-triazole				35.5%	14.2%	25.2±2.6	31.2	21
61	Me			S		359±69	26%	10.3±0.7	60±11	17
62	Bn			S		597±8	2110±740	155±33	87±7	17
63	3-MeBn			S		179±19	3610±1110	13.9±5.7	48±9	17
64	3-ClBn			S		91.8±6.0	995±206	6.7±0.4	62±3	17
65	3-IBn			S		45.9±2.1	575±75	1.9±0.4	60±4	17
66	Naphth-1-yl-Me			S		129±23	206±15	42.2±13.0	72±4	17
67		Cl		S	MeNHCO	89.2±11.7	158±29	0.40±0.06	100±5	18
68	3-IBn	Cl			MeNHCO	1240±320	5360±2470	1.4±0.3	100	14
69	3-IBn		NH_2		MeNHCO	3080±380	67%	137±41	37±5	20
70	3-IBn		CH_2NH_2		MeNHCO	52%	6%	1690±330	17±2	20

#	Substitution					AR binding affinity (nM)[a] or % displ. at 10 μM; A_3AR efficacy				Ref.
	R_1	R_2	R_3	R_4	R_5	K_i (hA_1AR)	K_i ($hA_{2A}AR$)	K_i (hA_3AR)	Efficacy (%)[b]	
71	3-IBn	Cl	N_3		MeNHCO	70%	29%	4270±1400	0	20
72	Me	Cl		S	MeNHCO	1330±240	20%	0.28±0.09	119±12	18
73	Me	Cl		S	diMeNCO	10%	12%	1500±1300	8.3±5.9	18
74	Me	Cl		S	cycloPrNHCO	47.8±5.7	2770±580	2.82±1.03	98±8	18
75	Me	Cl		S	*i*-PenNHCO	4070±1220	14%	1.63±0.17	92±4	18
76	Me	Cl		S	3-F-BnNHCO	67%	41%	17.4±3.8	57±2	18
77	Me	Cl		S	2-(3-F-Ph)EtNHCO	15%	30%	85.6±35.6	11±5	18
78	Me	Cl		S	3,3-diPhPrNHCO	20%	15%	415±16	0.1±2.8	18
79	cycloPr	Cl		S	MeNHCO	37.3±2.5	4890±380	2.24±1.21	99±3	18
80	cycloPr	Cl		S	EtNHCO	3.2±0.3	604±110	0.67±0.07	97±3	18
81	cycloPr	Cl		S	4-Bn-piperidineCO	32%	33%	4020±740	0	18
82	cycloPen	Cl		S	EtNHCO	2.0±2	149±29	2.83±0.63	95±3	18
83	2-MeBn	Cl		S	EtNHCO	75.8±2.5	429±97	2.50±1.10	112±9	18
84	2-MeBn	Cl		S	diMeNCO	0%	22.5%	632±70	9.1±0.4	18
85	3-IBn	Cl		S	EtNHCO	144±55	292±120	0.89±0.18	100±6	18
86	3-IBn	Cl		S	cycloPrNHCO	92.0±10.9	326±23	2.96±1.03	87±4	18
87	3-IBn	Cl		S	cycloBuNHCO	126±2	549±78	18.2±13.4	100±3	18
88	3-IBn	Cl		S	4-(4-F-Ph)-PiperazineCO	24%	12%	1440±830	96±10	18
89	3-IBn	Cl		S	3-ClBnNHCO	1710±340	28%	308±148	33±9	18
90	3-IBn	Cl		S	PhEtNHCO	20%	11%	433±141	7.1±2.7	18
91	3-IBn	Cl		S	3,3-diPhPrNHCO	5%	3%	343±48	31±14	18

a) AR experiments were generally performed using adherent CHO cells stably transfected with cDNA encoding the human ARs. Percent activation of the human A_3AR was determined at 10 μM. Binding at human A_1 and A_{2A}ARs in this study was carried out using [^{3}H]R-PIA (N^6-[(R)-phenylisopropyl]adenosine) or [^{3}H]CGS 21680 (2-[p-(2-carboxyethyl)phenyl-ethylamino]-5′-*N*-ethylcarboxamidoadenosine) as a radioligand. Binding at human A_3AR was carried out using [^{125}I]I-AB-MECA as a radioligand. Values from the present study are expressed as mean ± s.e.m., n = 3-5.

b) Percent A_3AR activity at 10 μM, relative to the ability of 10 μM Cl-IB-MECA to inhibit adenylyl cyclase.

ND: not determined.

Table II. Measured and predicted binding affinities and relative maximal agonist efficacy of adenosine derivatives at human A_3ARs in the training set. Refer to Figure 1A for structures of the adenosine derivatives. Affinities were previously reported.[14-21,39]

#	pK_i at hA_3AR	Predicted binding affinities (pK_i)								Efficacy (%)	Predicted Eff. (%)
		CoMFA-2	CoMFA-1	CoMFA-RF2	CoMFA-RF1	CoMFA-HB2	CoMFA-HB1	CoMSIA-2	CoMSIA-1		
1	6.54	7.36	7.35	7.16	7.25	7.47	7.20	7.76	7.71	100	107
2	7.06	7.53	7.43	7.33	7.24	7.52	7.28	7.51	7.43	100	97.5
3	6.81	6.96	6.80	6.87	6.72	6.78	6.79	6.82	6.79	75.2	103
4	6.25	6.54	6.50	6.60	6.39	6.51	6.69	6.49	6.52	99.1	99.5
5	6.34	6.13	6.28	6.26	6.27	6.51	6.65	6.20	6.25	101	102
6	6.65	6.79	6.87	6.74	6.92	6.71	6.79	6.85	6.86	92.8	79.3
7	7.07	6.84	6.91	6.71	6.91	6.67	6.85	6.74	6.74	108	89.2
8	6.91	6.83	6.86	6.75	6.92	6.73	6.80	6.93	6.92	43.7	66.3
9	6.44	6.54	6.44	6.50	6.55	6.52	6.65	6.18	6.21	32.2	34.3
10	6.93	6.91	6.96	6.99	6.81	6.85	6.79	6.97	6.91	16.9	5.90
11	7.27	6.87	6.91	6.73	6.92	6.83	6.96	6.93	6.96	70.7	67.0
12	6.67	6.75	6.75	6.73	6.80	6.86	6.82	6.89	6.89	7.30	38.9
13	6.62	6.73	6.78	6.72	6.82	7.01	6.94	7.00	7.01	70.9	65.1
14	6.33	6.76	6.71	6.74	6.78	6.82	6.81	6.82	6.83	95.5	77.1
15	6.03	6.18	6.17	6.62	6.44	6.45	6.45	6.39	6.39	3.60	20.8
16	6.64	6.85	6.82	6.81	6.82	6.75	6.77	6.57	6.58	85.1	72.1
17	6.98	7.02	6.96	6.77	6.92	7.11	6.89	6.88	6.88	91.9	78.6
18	6.84	6.81	6.75	6.76	6.74	6.86	6.80	6.97	6.98	1.40	12.5
19	7.39	7.04	7.01	6.79	6.91	6.78	6.79	7.16	7.17	31.0	34.5

20	6.94	6.92	6.88	6.74	6.89	7.06	6.80	6.82	6.84	69.0	65.8
21	6.69	6.72	6.70	6.69	6.78	6.79	6.78	6.71	6.70	12.8	26.9
22	7.27	7.27	7.28	7.11	7.27	7.18	7.13	7.31	7.33	0	2.12
23	6.51	6.35	6.37	6.58	6.42	6.36	6.28	6.33	6.28	72.0	55.4
24	7.80	7.60	7.56	7.26	7.47	7.55	7.58	7.52	7.51	100	107
25	6.35	7.51	7.40	7.45	7.19	7.43	7.70	***7.92***	***8.10***	0	***71.0***
26	8.03	7.77	7.89	7.57	7.94	8.11	7.95	8.20	8.17	96.0	101
27	7.54	7.67	7.70	7.39	7.58	7.48	7.50	7.40	7.44	107	98.7
28	8.33	7.98	7.94	7.82	8.07	7.45	7.54	7.84	7.83	102	89.9
29	7.74	7.58	7.51	7.50	7.53	7.64	7.29	7.64	7.61	111	91.9
30	5.42	5.17	5.13	5.28	5.24	5.74	5.85	5.51	5.53	21.0	18.7
31	7.14	7.42	7.31	7.43	7.21	7.54	7.18	7.32	7.32	99.0	100
32	6.04	6.04	5.93	6.14	6.22	6.73	6.50	5.79	5.74	23.0	20.8
33	7.99	7.68	7.80	7.61	7.88	7.73	7.80	7.95	7.97	108	105
34	7.83	7.74	7.83	7.53	7.87	7.15	7.58	7.90	7.93	102	102
35	7.38	7.76	7.68	7.70	7.58	7.73	7.74	7.59	7.68	55.0	93.9
36	8.68	8.65	8.78	8.67	8.86	8.55	8.45	8.68	8.69	84.0	92.9
37	7.05	7.01	6.87	7.17	6.89	7.24	7.26	6.79	6.81	73.0	63.1
38	7.33	7.29	7.43	7.04	7.56	7.27	7.50	7.34	7.37	100	93.0
39	7.49	8.00	7.82	7.71	7.97	7.55	7.51	7.56	7.59	81.0	86.5
40	7.76	7.81	7.82	7.51	7.89	7.64	7.47	7.85	7.84	95.0	110
41	8.36	8.02	7.94	7.85	7.89	7.83	7.78	7.71	7.72	80.0	92.4
42	7.32	7.81	7.67	7.75	7.59	7.75	7.72	7.47	7.51	96.0	99.0
43	8.06	7.89	7.90	7.98	7.98	8.06	7.77	7.98	7.98	102	89.1
44	7.17	7.11	7.11	7.51	7.31	7.29	7.30	7.31	7.37	97.0	92.3

45	9.20	9.16	9.14	9.12	9.21	8.62	8.48	8.92	8.95	117	119
46	7.62	7.86	7.72	8.17	7.81	7.80	7.71	7.88	7.86	87.0	78.3
47	8.04	8.43	8.26	8.60	8.33	8.62	8.33	8.42	8.49	99.0	90.8
48	8.41	8.22	8.28	7.94	8.25	8.05	8.13	8.27	8.18	0	2.38
49	6.97	6.89	6.89	7.15	7.12	6.91	7.05	7.19	7.13	0	-3.84
50	9.04	8.99	8.94	8.85	9.04	8.86	8.76	9.03	8.94	99.0	*41.8*
51	6.94	6.85	6.73	7.48	7.04	6.49	6.73	6.88	6.83	98.0	90.7
52	8.31	7.74	7.70	7.66	8.09	7.54	7.86	7.74	7.87	64.0	61.2
53	8.47	8.42	8.47	8.29	8.22	8.21	8.41	8.19	8.19	101	103
54	7.41	7.69	7.62	7.54	7.64	7.48	7.31	7.31	7.32	98.0	99.1
55	7.97	8.13	8.08	7.80	7.94	8.06	8.00	7.83	7.81	83.7	81.4
56	8.82	8.41	8.68	8.37	8.16	8.36	8.28	***7.53***	***7.47***	9.40	10.6
57	7.48	7.26	7.47	8.34	7.99	8.06	8.14	7.57	7.55	0	-3.63
58	7.83	7.62	7.81	8.00	7.50	7.74	7.91	7.82	7.75	14.0	19.5
59	8.02	8.00	8.13	8.21	7.70	8.05	8.04	8.09	8.01	0	-6.68
60	7.60	7.37	7.58	7.97	7.50	7.65	7.73	7.61	7.52	31.2	24.7
61	7.99	7.93	7.93	7.88	7.87	7.88	8.05	8.35	8.55	60.0	64.2
62	6.81	7.60	7.63	7.71	7.48	7.76	7.92	7.72	***8.08***	87.0	68.7
63	7.86	7.82	7.86	7.84	7.76	7.86	8.09	7.77	8.05	48.0	65.1
64	8.17	7.81	7.87	7.83	7.79	7.85	8.08	7.86	8.13	62.0	66.8
65	8.72	7.76	7.87	7.78	7.77	7.82	8.06	8.00	8.12	60.0	64.4
66	7.37	7.41	7.34	7.43	7.27	7.57	7.92	7.53	7.71	72.0	***3.63***
67	9.40	8.93	8.91	8.69	9.05	8.66	9.20	8.86	8.84	100	99.2
68	8.85	8.23	8.46	7.91	8.56	8.48	8.40	***7.62***	***7.54***	100	90.8
69	6.86	6.95	7.24	7.16	7.28	7.31	7.45	7.23	7.19	37.0	***99.5***

70	5.77	5.83	5.57	6.11	5.49	5.34	5.48	5.70	5.68	17.0	13.3
71	5.37	5.85	5.62	6.32	5.35	5.28	5.51	5.32	5.28	0	-6.47
72	9.55	9.45	9.37	9.24	9.52	9.35	9.34	9.37	9.36	119	94.6
73	5.82	6.44	6.45	6.35	5.91	6.56	6.38	*7.63*	*7.57*	8.30	28.2
74	8.55	8.74	8.76	8.81	8.64	8.87	8.64	8.93	8.95	98.0	108
75	8.79	8.94	8.88	8.41	8.85	8.38	8.41	9.01	8.97	92.0	97.0
76	7.76	7.51	7.46	7.81	7.34	7.37	7.46	7.42	7.46	57.0	48.0
77	7.07	7.04	6.78	7.02	6.99	6.62	6.65	6.99	7.02	11.0	9.32
78	6.38	6.39	6.18	6.31	6.28	6.24	6.02	6.71	6.73	0.10	17.1
79	8.65	9.21	9.33	9.03	9.36	9.17	9.25	9.11	9.13	99.0	99.5
80	9.17	9.13	9.08	9.14	9.07	9.05	8.82	9.02	9.01	97.0	105
81	5.40	5.45	5.58	5.00	5.57	5.00	4.68	5.44	5.47	0	9.23
82	8.55	8.83	8.56	8.95	8.61	9.05	8.57	8.75	8.79	95.0	107
83	8.60	8.10	8.25	8.04	8.56	8.17	8.23	7.98	8.08	112	86.1
84	6.20	5.63	5.82	5.57	6.08	6.54	6.15	6.38	6.44	9.10	10.4
85	9.05	8.96	8.96	8.86	9.08	8.84	8.73	8.65	8.60	100	92.5
86	8.53	8.91	8.90	8.83	8.73	8.95	8.95	8.93	8.83	87.0	112
87	7.74	7.90	8.00	8.11	7.90	8.29	8.25	8.12	8.11	100	95.3
88	5.84	5.88	6.10	6.00	5.81	6.01	5.74	5.90	5.90	96.0	94.8
89	6.51	6.77	6.79	7.15	6.51	7.22	7.36	6.53	6.54	33.0	30.7
90	6.36	6.32	6.42	6.37	6.47	6.53	6.46	6.42	6.41	7.10	3.88
91	6.46	6.16	6.16	6.18	6.33	6.15	6.18	6.34	6.30	31.0	17.4

The numbers in bold italics indicate outliers in the residual plots from the cross-validation analyses.

Table III. The binding affinities of 25 adenosine derivatives (test set) at human (unless noted, r – rat) A_1, A_{2A}, and A_3ARs expressed in CHO cells (expressed as K_i value or percent inhibition at 10 μM) and relative maximal agonist efficacy at 10 μM at the A_3AR. Unless noted, R_1, R_2 = H; R_3 = OH; R_4 = O; R_5 = CH_2OH.

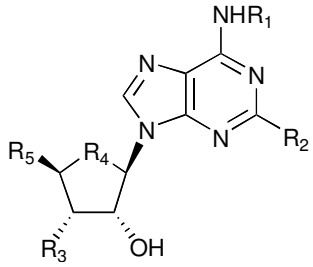

#	Substitution					AR binding affinity (nM)[a] or % displ. at 10 μM; A_3AR efficacy				Ref.
	R_1	R_2	R_3	R_4	R_5	K_i (hA_1AR)	K_i ($hA_{2A}AR$)	K_i (hA_3AR)	Efficacy (%)[b]	
92	3-IBn					7.4±1.7	135±22	5.8±0.4	46±8	15
93	(*S*)-2-Ph-1-Pr					26.6±6.8	1120±260	38.8±4.1	98±6	14
94	cyclooctyl					1.7±0.1 (r)	6200±1120 (r)	411±55	49±5	19
95		3-ClBnO				27.4±3.9	228±66	71.6±24.6	16.2±3.8	16
96		2-FPhEtO				331±22	58.1±24.9	77.8±13.5	44.5±5.1	16
97		4-FPhEtO				467±100	56.8±16.3	112±16	73.4±5.2	16
98		3,4-DiMeOPhEtO				469±118	30.3±2.8	863±313	66.5±3.7	16
99		PhBuO				1100±230	243±166	251±80	19.3±6.2	16
100		PhPenO				700±126	249±54	429±159	9.8±8.8	16
101	Me	4-PrPhC≡C				45.4%	2.9%	4.5±0.9	0	21
102	Me	4-Bu-triazol				848±76	23.0%	11.7±3.1	3.4	21
103	Me	4-pyridinyl-triazol				1970±210	39.7%	10.3±1.5	11.4	21
104	5-Cl-2-MeOBn	CN				63.2±16.9	1260±190	2.76±0.51	29±6	15

105	PhEt			S		82.6±6.8	507±31	5.6±1.1	86±5	13
106	3-IBn		N_3		MeNHCO	64%	32%	2260±480	0	20
107	Me	Cl		S		629±168	4%	0.8±0.1	96±5	17
108	Bn	Cl		S		2280±180	47%	18.2±2.6	63±4	17
109	2-MeBn	Cl		S		853±133	3280±170	48.9±16.6	62±4	17
110	3-IBn	Cl		S		554±64	1190±290	3.2±0.9	32±7	17
111	Me	Cl		S	4-Bn-piperidineCO	10%	6%	3500±340	3.1±1.3	18
112	cycloPr	Cl		S	cycloPrNHCO	4.6±0.3	325±13	5.56±1.77	85±4	18
113	cycloPr	Cl		S	morpholineCO	25%	11%	4440±160	83±5	18
114	cycloPen	Cl		S	MeNHCO	13.9±18	921±76	4.27±0.33	105±2	18
115	2-MeBn	Cl		S	cycloPrNHCO	76.7±9.3	202±51	27.8±3.8	91±3	18
116	3-IBn	Cl		S	MeNHCO	193±46	223±36	0.38±0.07	114±9	18

a) AR experiments were generally performed using adherent CHO cells stably transfected with cDNA encoding the human ARs. Percent activation of the human A_3AR was determined at 10 μM. Binding at human A_1 and A_{2A}ARs in this study was carried out using [^{3}H]R-PIA or [^{3}H]CGS 21680 as a radioligand. Binding at human A_3AR was carried out using [^{125}I]I-AB-MECA as a radioligand. Values from the present study are expressed as mean ± s.e.m., n = 3-5.

b) Percent A_3AR activity at 10 μM, relative to the ability of 10 μM Cl-IB-MECA to inhibit adenylyl cyclase.

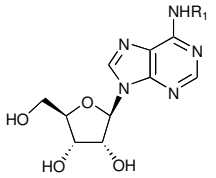

1, 26 - 50, 92 - 94

R_1 =

Ź H
26 CH_3
27 CH_3O
28 C_2H_5
29 $(CH_3)_2CH$
30 $((CH_3)_2CH)_2CH$
31 cyclopentyl
32 (*S*)-*endo*-norbornyl
33 cyclopropyl-CH_2
34 Ph
35 Bn
36 $Ph(CH_2)_2$
37 $Ph(CH_2)_2O$

R_1 =

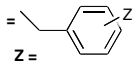

Z =

38 2-CH_3
39 2-CH_3O
40 2-Cl
41 3-Cl
42 4-Cl

R_1 =

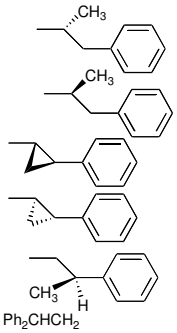

43
44
45
46
47
48 Ph_2CHCH_2

49

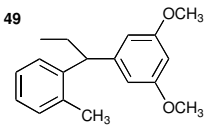

50

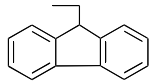

92 3-I-Bn

93

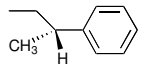

94 cyclooctyl

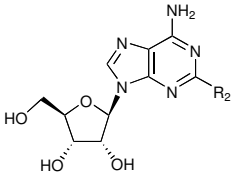

2 - 23, 95 - 100

R_1 =

2 Cl
3 CH_3O
4 C_2H_5O
5 $(CH_3)_2CHO$
6 $CH_3(CH_2)_4O$
7 $(CH_3)_2CHCH_2O$
8 $CH_3(CH_2)_5O$
9 PhO
10 BnO
11 $Ph(CH_2)_2O$
12 2-CH_3-$Ph(CH_2)_2O$
13 3-CH_3-$Ph(CH_2)_2O$
14 4-CH_3-$Ph(CH_2)_2O$
15 2-CH_3O-$Ph(CH_2)_2O$
16 3-CH_3O-$Ph(CH_2)_2O$
17 4-CH_3O-$Ph(CH_2)_2O$
18 2-Cl-$Ph(CH_2)_2O$
19 3-Cl-$Ph(CH_2)_2O$
20 4-Cl-$Ph(CH_2)_2O$
21 1-naphthyl-$(CH_2)_2O$
22 Ph_2CHCH_2O
23 $Ph(CH_2)_2NH$
95 3-Cl-BnO
96 2-F-$Ph(CH_2)_2O$
97 4-F-$Ph(CH_2)_2O$
98 3,4-$(MeO)_2$-$Ph(CH_2)_2O$
99 $Ph(CH_2)_4O$
100 $Ph(CH_2)_5O$

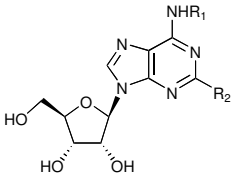

53 - 60, 101 - 104

R_1 = CH_3, R_2 =

53 CN
54 NH_2
55 N_3
56 4-CH_3 -Ph-ethynyl
57 4-$CH_3(CH_2)_4$ -Ph-ethynyl

58

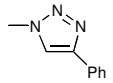

59

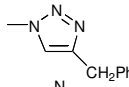

60

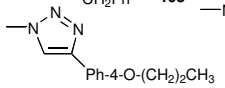

101 4-$CH_3(CH_2)_2$-Ph-ethynyl

102

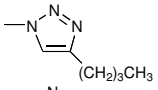

103

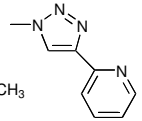

104 R_2 = CN, R_1 =

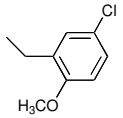

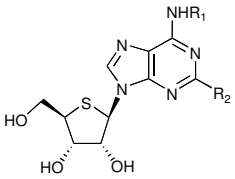

25, 52, 61 - 66, 105, 107 - 110

25 R_1, R_2 = H
52 R_1 = H, R_2 = Cl

R_2 = H, R_1 =

61 CH_3
62 Bn
63 3-CH_3-Bn
64 3-Cl-Bn
65 3-I-Bn

66

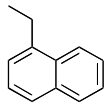

105 $Ph(CH_2)_2$

R_2 = Cl, R_1 =

107 CH_3
108 Bn
109 3-Cl-Bn
110 3-I-Bn

Figure I-A.

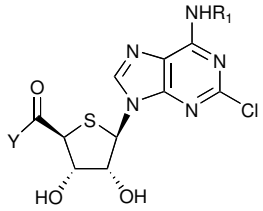

67, 72- 91, 111 - 116

67 R_1 = H, Y = CH_3NH

R_1 = CH_3, Y =

72 CH_3NH

73 $(CH_3)_2N$

74 cyclopropyl-NH

75 $(CH_3)_2CH(CH_2)_2NH$

76 3-F-Bn-NH

77 3-F-Ph$(CH_2)_2$-NH

78 $Ph_2CH(CH_2)_2$-NH

R_1 = cyclopropyl, Y =

79 CH_3NH

80 C_2H_5NH

81

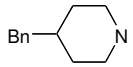

82 R_1 = cyclopentyl, R_2 = C_2H_5NH

83 R_1 = 2-CH_3-Bn, R_2 = C_2H_5NH

84 R_1 = 2-CH_3-Bn, R_2 = $(CH_3)_2N$

R_1 = 3-I-Bn, Y =

85 C_2H_5NH

86 cyclopropyl-NH

87 cyclobutyl-NH

88

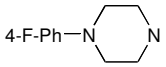

89 3-Cl-Bn-NH

90 $Ph(CH_2)_2$-NH

91 $Ph_2CH(CH_2)_2$-NH

111 R_1 = CH_3, Y =

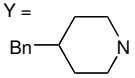

112 R_1 = cyclopropyl, Y = cyclopropyl-NH

113 R_1 = cyclopropyl, Y =

114 R_1 = cyclopentyl, Y = CH_3NH

115 R_1 = 2-CH_3-Bn, Y = cycloproyl-NH

116 R_1 = 3-I-Bn, Y = CH_3NH

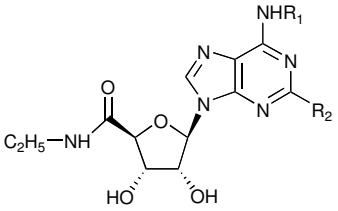

24, 51

24 R_1, R_2 = H

51 R_1 = H, R_2 =

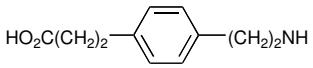

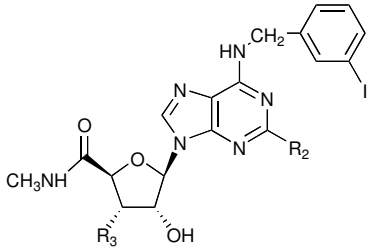

68 - 71, 106

68 R_2 = Cl, R_3 = OH

69 R_2 = H, R_3 = NH_2

70 R_2 = H, R_3 = CH_2NH_2

71 R_2 = Cl, R_3 = N_3

106 R_2 = H, R_3 = N_3

Figure I-B.

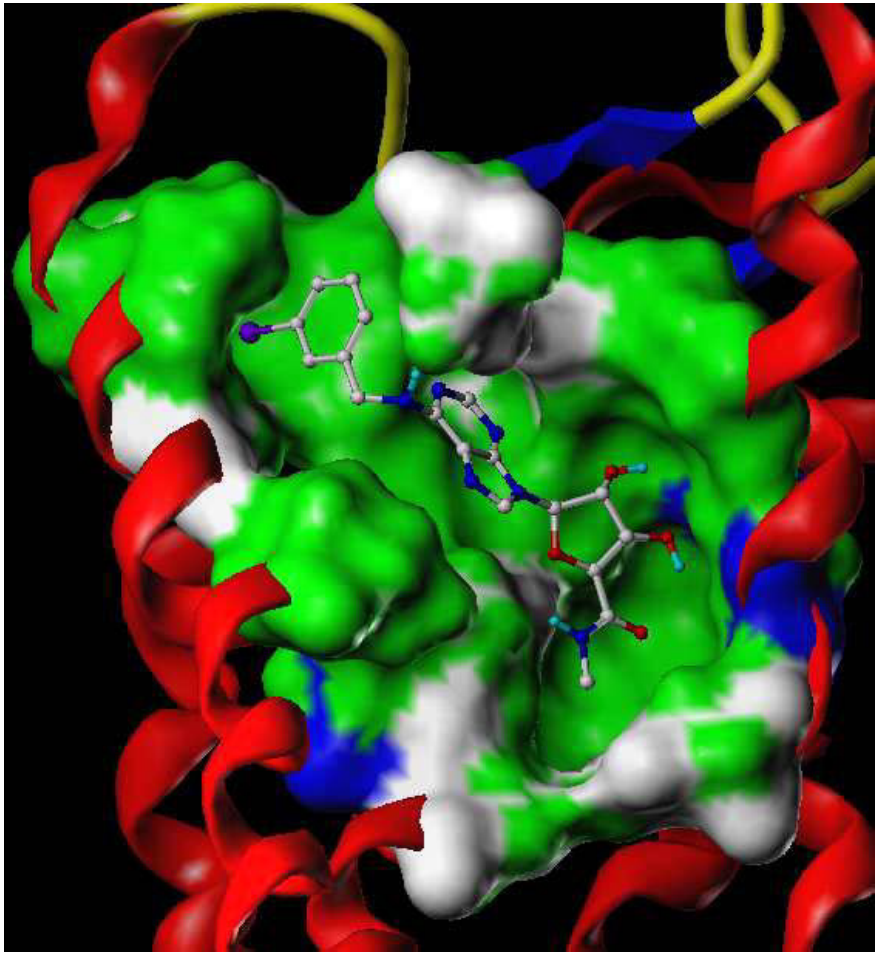

Figure II.

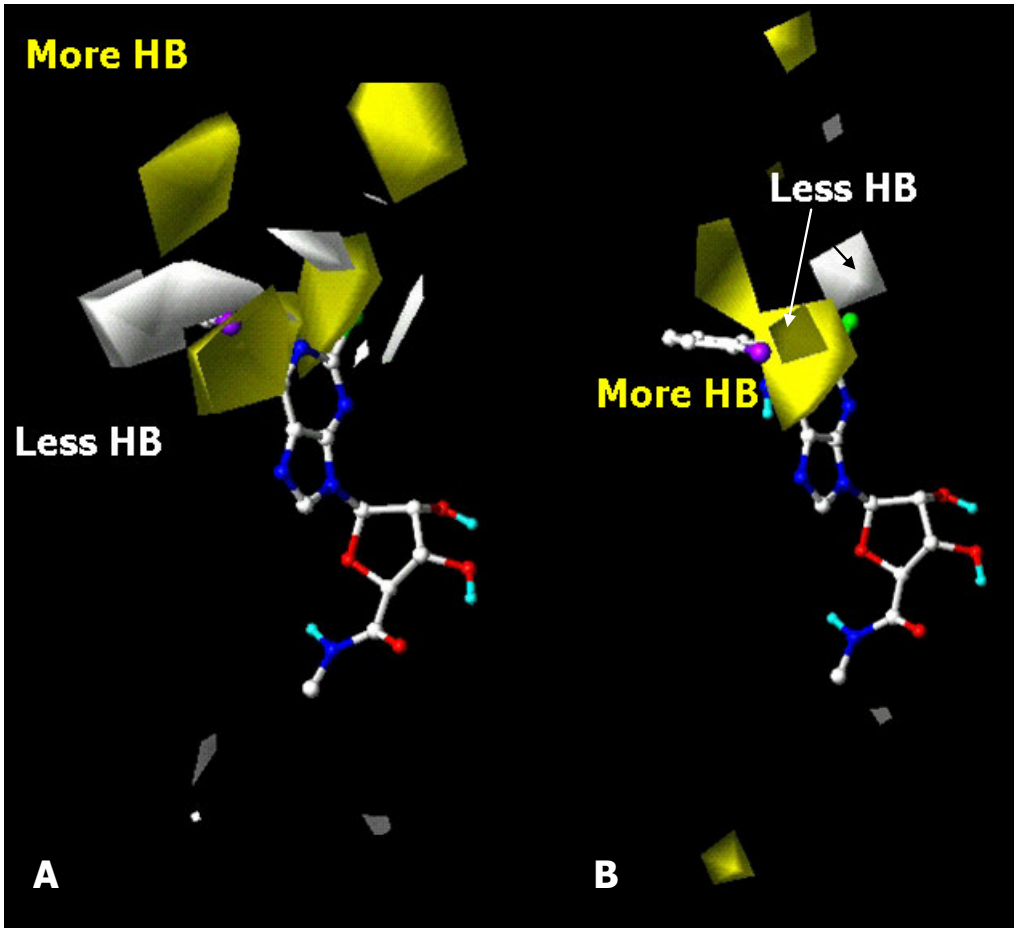

Figure III.